Journal of Volcanology and Geothermal Research 267 (2013) 57–67

Contents lists available at ScienceDirect

Journal of Volcanology and Geothermal Research

journal homepage: www.elsevier.com/locate/jvolgeores

Seismicity, Vp/Vs and shear wave anisotropy variations during the 2011 unrest at Santorini caldera, southern Aegean

K.I. Konstantinou [a,*], C.P. Evangelidis [b], W.-T. Liang [c], N.S. Melis [b], I. Kalogeras [b]

[a] Dept of Earth Sciences, National Central University, Jhongli 320, Taiwan
[b] Institute of Geodynamics, National Observatory of Athens, POB 20048, 11810 Athens, Greece
[c] Institute of Earth Sciences, Academia Sinica, POB 1-55, Taipei 115, Taiwan

ARTICLE INFO

Article history:
Received 13 May 2013
Accepted 1 October 2013
Available online 10 October 2013

Keywords:
Santorini
Caldera unrest
Stress
Shear wave splitting
Aegean

ABSTRACT

The Santorini caldera has been the focus of several large explosive eruptions in the past, the last of which occurred in the early 1950s. The volcano was dormant until early 2011 when increasing number of earthquakes accompanied significant intra-caldera uplift. This seismic activity was recorded by 8 temporary as well as 19 permanent seismic stations that were installed on Santorini and nearby islands after the onset of the unrest. Using data from January 2011 until June 2012 we calculated accurate relative locations for 490 events utilizing both catalog and waveform cross-correlation differential travel times of P- and S-phases. The distribution of relocated events exhibits a large cluster between Thera and Nea Kameni islands along the caldera rim, suggesting the activation of a preexisting ring fault. All hypocenters are located between 5 and 11 km resulting in a sharp cutoff of seismicity above and below these depths. We also used P and S travel times in order to calculate average Vp/Vs ratios and estimated shear wave splitting parameters (fast direction φ, delay time δt) for events within the shear wave window. The Vp/Vs ratios at several stations exhibit a majority of values consistently below the regional one (~1.77). Their temporal variations can be explained as periods of gas influx and depletion in the upper crust beneath the caldera. A comparison of δt for a number of earthquake doublets shows a progressive decrease of delay times towards the end of the unrest probably as a result of cracks closing owing to stress relaxation. The seismological observations presented here are compatible with petrological models that suggest the existence of a deep (11–14 km) dacitic magma reservoir and a shallower (<5 km) rhyolitic magma chamber.

1. Introduction

Caldera unrest is a feature frequently observed at large silicic centers and heralds the onset of a new phase in their activity which may or may not be followed by an eruption (Newhall and Dzurisin, 1988). A salient characteristic of such unrest is deformation that is expressed through significant uplift rates within the caldera and is usually interpreted as the accumulation of magma and/or exsolved volatiles at depth. This is accompanied in most cases by a large number of microearthquakes as well as increased influx of gas leading to geochemical anomalies in fluid composition. In many instances the intensity of these phenomena after reaching a climax progressively dissipates, resulting in subsidence and decreasing seismicity rates. Well-studied examples of caldera unrest include Campi Flegrei in Italy (Carlino and Somma, 2010 and references therein) and Long Valley, California (e.g. Hill et al., 2003) where seismological, geodetic and geochemical observations were jointly analyzed. These two examples also vividly highlight the problem of trying to predict whether a large eruption is imminent and how it would affect densely populated areas around the caldera.

The Santorini caldera lies in the southern Aegean and was formed after several cycles of explosive volcanic activity over the last 400 ka (Fig. 1) (Bond and Sparks, 1976; Heiken and McCoy, 1984; Druitt and Francaviglia, 1992; Vougioukalakis and Fytikas, 2005). The last of these cycles started with a large eruption that occurred in the Late Bronze Age (about 1628 BC) involving hydrovolcanic activity and producing pyroclastic flows that destroyed early human settlements on the nearby islands. The eruption and its consequences are often blamed for the rapid demise of the thriving until then Minoan civilization of Crete. After this eruption several smaller ones followed in 197 BC, 1707, 1866, 1925, 1939 and 1950 AD according to the Global Volcanism Database of the Smithsonian Institution (http://www.volcano.si.edu). The small islands of Palea and Nea Kameni that lie in the center of the flooded caldera were created by this activity and are also thought to be the possible sites of future eruptions (Pyle and Elliott, 2006). Thera, the largest and most populated island in the Santorini complex, will be particularly vulnerable to hazards stemming from a future eruption such as ashfall, ballistic projectiles and toxic gas

* Corresponding author.
E-mail address: kkonst@ncu.edu.tw (K.I. Konstantinou).

0377-0273/$ – see front matter © 2013 Elsevier B.V. All rights reserved.
http://dx.doi.org/10.1016/j.jvolgeores.2013.10.001

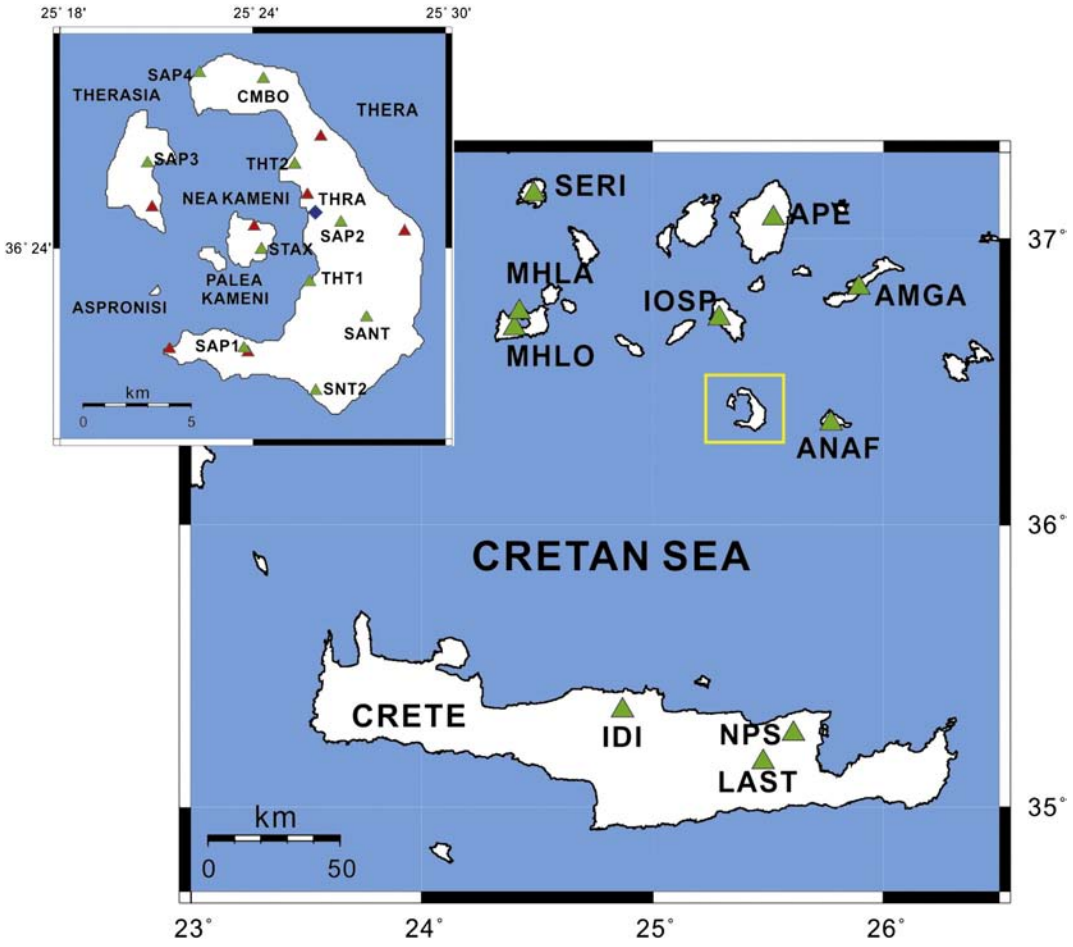

Fig. 1. Map of the southern Aegean where the location of the Santorini island complex is highlighted with a yellow square. The inset at the left hand side of the map shows an enlarged map of the five islands comprising the island complex. Seismic stations are shown as triangles, where the green color signifies three-component broadband instruments while the red color represents vertical component ones. The blue diamond corresponds to station THRA which is a three-component accelerometer located in the town of Fira. (For interpretation of the references to color in this figure legend, the reader is referred to the web version of this article.)

release. This situation is exacerbated by the fact that Santorini is a favorite tourist destination and attracts hundreds of thousands of visitors every year.

Since its last eruption in 1950 the volcanic system has been relatively quiet and the only observed activity was the emission of low-temperature hydrothermal fluids and occurrence of sporadic micro-earthquakes (Dimitriadis et al., 2009). This apparent quiescence ended in early 2011 when seismicity rates steadily increased above background levels (Chouliaras et al., 2012) and significant deformation in the form of uplift was detected in the permanent GPS stations around the caldera. Several studies have analyzed and interpreted the geodetic observations (GPS and InSAR) covering the time period from the start of the unrest in January 2011 until the end of 2012 (Newman et al., 2012; Parks et al., 2012; Foumelis et al., 2013; Lagios et al., 2013; Papoutsis et al., 2013). The concept of a Mogi source was used in order to identify the point of maximum uplift and all of the aforementioned authors generally agree that this point is located within the flooded caldera, to the north of Nea Kameni island at a depth of about 4 km. The deformation rates were estimated between 140 and 180 mm yr^{-1} corresponding to a volume rate of accumulated material in the range of 6×10^6 m^3 and 24×10^6 m^3 per year. Maps of the seismicity that accompanied the deformation were published in the aforementioned studies showing one large cluster of events extending from Thera to Palea Kameni in a NE–SW orientation, without however, providing any depth estimates. These locations were extracted from the seismicity catalogs of the Aristotle University of Thessaloniki and the National Observatory of Athens.

In this work, we focus on the seismological characteristics of the 2011 unrest placing special emphasis on (a) shear wave anisotropy which has been used successfully in the past as an indicator of the state of stress in a volcanic system (Gerst and Savage, 2004; Savage et al., 2010; Unglert et al., 2011) and (b) the Vp/Vs ratio whose variations may provide information about the elastic rock properties. We first give an overview of available data and then embark on obtaining accurate locations of events that occurred during the unrest using catalog as well as differential travel times from waveform cross-correlation. Based on these locations estimated travel times are used to calculate ratios of Vp/Vs and their temporal variation is constructed. Shear wave splitting parameters (fast polarization direction and delay time) are also estimated from observed S-phase waveforms. The temporal variation of splitting parameters is investigated by identifying event doublets that have occurred at different times within the study period. Finally, all these results are interpreted in conjunction with the geodetic/geochemical observations and a plausible scenario that explains these temporal and spatial variations is discussed.

2. Data and earthquake locations

Prior to the 2011 unrest SANT was the only permanent three-component seismic station on Santorini equipped with a broadband

STS-2 sensor that was deployed by GFZ-Potsdam as part of the GEOFON project in collaboration with the Institute of Geodynamics, National Observatory of Athens (IGNOA) (Fig. 1 inset). Additionally, a three-component strong-motion sensor (THRA) was also installed at the town of Fira as part of the nationwide strong-motion network operated by IGNOA. After the unrest had begun seven temporary stations equipped with three-component sensors were deployed by IGNOA either on Santorini or on nearby islands (SAP1-4, IOSP, AMGA, ANAF) augmented by permanent stations (MHLA, MHLO, NPS, LAST, IDI, APE). These were combined with seismic stations from the Aristotle University of Thessaloniki, seven only with vertical components and four with three-component sensors. All stations were provided with absolute timing through GPS receivers and operated under the framework of the Hellenic Unified Seismic Network (HUSN).

Our analysis starts with the manual picking of P- and S-phases of all events that were recorded by at least 4 stations from January 2011 until June 2012. Initial locations were then obtained by using HYPO2000 (Klein, 2002) and utilizing the minimum 1D velocity model of Dimitriadis et al. (2009) which was derived for the broader area of Santorini. It can be seen that these locations form a NE–SW cluster within the caldera with many events scattered around it, similar to the seismicity maps published previously (Fig. 2). In order to improve the accuracy of these initial locations, we used the COMPLOC package that applies a shrinking grid-search relocation algorithm using source specific station corrections (Lin and Shearer, 2006). The method accepts as input the initial location of events and their corresponding travel times, calculates iteratively station corrections for each source–receiver pair and inverts for a new set of locations. These source specific station terms are the weighted median of residuals at a given station from nearby events. The number of nearby events (N) and the maximum allowed distance are defined and reduced in subsequent iterations. In our case, it starts with 500 events and a maximum cutoff distance of 50 km and is reduced after 15 iterations to 20 nearby events and 2 km distance. This relocation procedure is expanded by adding also differential travel times from waveform cross-correlation (CC). The differential travel times are included as additional information to the observed arrival times in order to solve for a new set of adjusted picks by minimizing the misfit of both the observed picks and the differential times. In order to identify similar event clusters required for this operation, we follow the cluster analysis method proposed by Shearer et al. (2005). This relocation methodology has been used in both large scale studies covering southern California, but also in volcanic areas where the spatial scale is considerably smaller (Hawaii Island, Matoza et al., 2013).

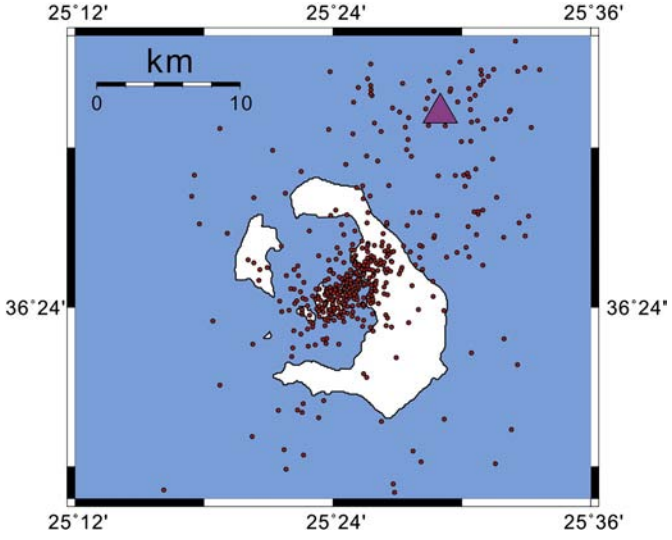

Fig. 2. Map showing the initial locations of local events from January 2011 until June 2012 estimated after inversion of the corresponding P- and S-phase arrival times. The purple triangle to the NE of Thera island signifies the location of the Coloumbo submarine volcano (see text for more details). (For interpretation of the references to color in this figure legend, the reader is referred to the web version of this article.)

For the application of this methodology to the Santorini dataset we include both catalog and differential travel times using the minimum 1-D velocity model of Dimitriadis et al. (2009) as before. Differential travel times are obtained after low-pass filtering of the waveforms at 5 Hz and using a time window of 1 second around the P-phase and 1.5 s around the S-phase. The choice of the filter cutoff at 5 Hz was based on tests we performed using different frequency bands. Moreover, the study of ambient noise level in Greece (Evangelidis and Melis, 2012) has shown elevated levels of high frequency noise in station SANT. Therefore, such a low-pass filtering minimizes the cultural noise considerably. Waveforms of event pairs are cross-correlated at stations with epicentral distances that do not exceed 150 km, even though it has to be noted that the majority of the events were recorded only by the stations on Santorini islands owing to their small magnitudes. For each event pair waveforms at each station were cross-correlated and a value that is the average of the P- and the S-phase CC coefficient is considered the CC value for this pair. An event pair is defined when there are at least three differential measurements for two events. Moreover, closely spaced events with average CC values higher than 0.65 define an event cluster. The choice of these values is a compromise between the highest relocation precision and the largest possible number of events that can be assigned to a cluster (Shearer et al., 2003). In this way, a total of 490 events were finally relocated and assigned into 23 clusters.

In general, we find that P-phases have more event pairs with a higher CC coefficient than the S-phases implying contamination of the S-wave onset by the P-wave coda (Fig. 3a). Also the distribution of the number of stations with average CC coefficients higher than 0.55 exhibits a peak around 6 and this happens mostly at station SANT and the vertical component stations on Santorini islands that were recording events from the initiation of the unrest (Fig. 3b,c). We estimate relative location uncertainties using a bootstrap technique where random errors, drawn from a normal distribution, are added to the differential times and each event is relocated 200 times (Shearer, 1997). This procedure will result in a cloud of locations for whose horizontal and vertical scatter can be utilized in order to estimate formal errors. The mean values for the relative horizontal and vertical bootstrap errors are found to be 1.0 km and 0.7 km respectively (Fig. 4).

Fig. 5 shows a map with the distribution of all the relocated events in and around the Santorini caldera, while three depth cross-sections can be seen in Fig. 6. As expected, most of the seismicity occurs inside the caldera where a large cluster of events appears between the islands of Thera and Nea Kameni and smaller clusters can also be found beneath both Kameni islands. The depth cross-section CC′ indicates that the large cluster actually consists of two smaller clusters, a deeper one that is vertical and a shallower one that exhibits some dipping towards the caldera. A number of events are also located to the NE offshore of Thera, around the area where the Coloumbo submarine volcano is situated. Coloumbo is an active volcanic system that last erupted in 1650 AD and it is characterized by intense, high-temperature (~220 °C) fumarolic activity and seismicity (Dimitriadis et al., 2009; Konstantinou and Yeh, 2012), therefore the appearance of events there can be considered as usual and not as the result of unrest in the caldera. The hypocentral depths of the events within the caldera are distributed from a maximum depth of about 11 km to a depth as shallow as 5 km. The earthquakes located around Coloumbo seem to be an exception to this trend, as their depth range is somewhat deeper between 9 and 13 km. The two locations of the Mogi source of deformation, one obtained by most authors (Newman et al., 2012; Parks et al., 2012; Foumelis et al., 2013; Lagios et al., 2013) and the other by Papoutsis et al. (2013) do not coincide exactly with the large cluster of events. The temporal evolution of seismicity during the unrest is shown with a

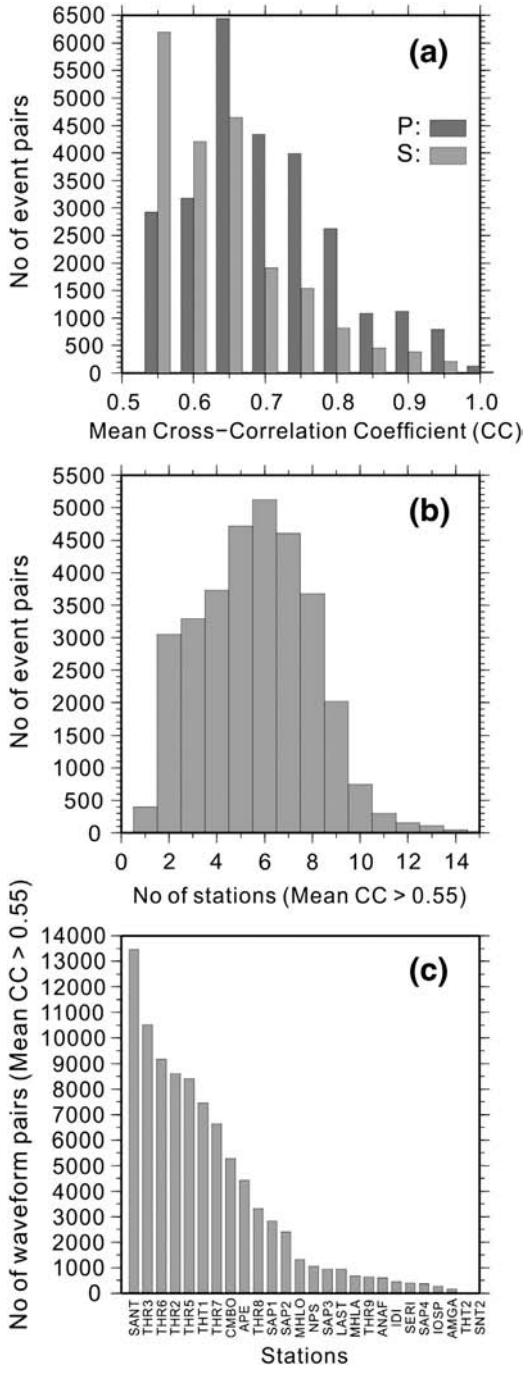

Fig. 3. Histograms showing (a) the distribution of cross-correlation coefficients for P- and S-phases respectively, (b) the distribution of the number of stations that had an average cross-correlation coefficient (for P and S phases) higher than 0.55, and (c) the distribution of the number of waveform pairs with average cross-correlation coefficients higher than 0.55 at the different stations used in this study.

color scale in Fig. 6 and it can be seen that events occur mostly within the same clusters throughout the unrest period.

3. Estimation of Vp/Vs ratios

The ratio of compressional to shear wave velocity has been used in the past as a proxy for detecting variations in crustal rock properties due to the presence of fluids or changing crack geometry/distribution (e.g., Lin and Shearer, 2009; Lucente et al., 2010). For the events that are located within the Santorini caldera, we calculated an average

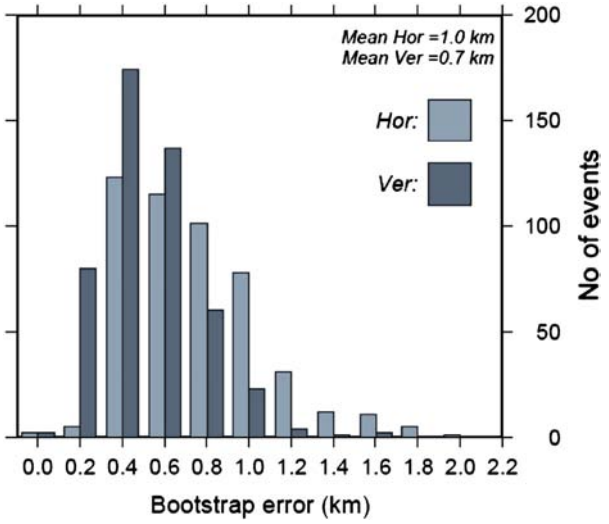

Fig. 4. Histogram showing the distribution of the bootstrap error for the relocated events in both the horizontal and vertical directions.

Vp/Vs ratio along the ray path from the estimated travel times at each station, following the approach of Nur (1972) where

$$V_p/V_s = t_s/t_p$$

where $t_s = T_s - T_o$ and $t_p = T_p - T_o$ where T_s and T_p are the arrival times of the S- and P-wave respectively and T_o is the origin time of each earthquake. Such an estimation is of course possible only for the three-component stations and Table 1 gives a list of these stations along with some statistics regarding the measurements. In total 440 Vp/Vs ratios in the range of 1.2–2.2 have been estimated at 6 stations and their overall average value is 1.54 ± 0.17 for the period between February 2011 and June 2012. Corresponding errors for each Vp/Vs ratio have been estimated by using the uncertainties of P- and S-phase picks. Two stations (THRA, SANT) have measurements that span almost

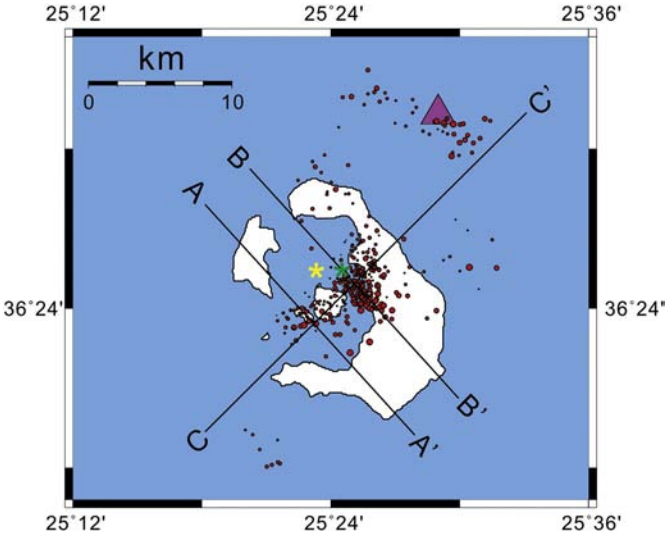

Fig. 5. Map showing the relative locations obtained after applying the grid-shrinking algorithm of Lin and Shearer (2006, 2009). The thick black lines represent the direction of the three depth cross-sections shown in the next figure. The yellow star indicates the location of the Mogi source estimated by Newman et al. (2012), Parks et al. (2012), Foumelis et al. (2013) and Lagios et al. (2013) while the green star is the Mogi source estimated by Papoutsis et al. (2013). All other symbols are the same as in Fig. 2. (For interpretation of the references to color in this figure legend, the reader is referred to the web version of this article.)

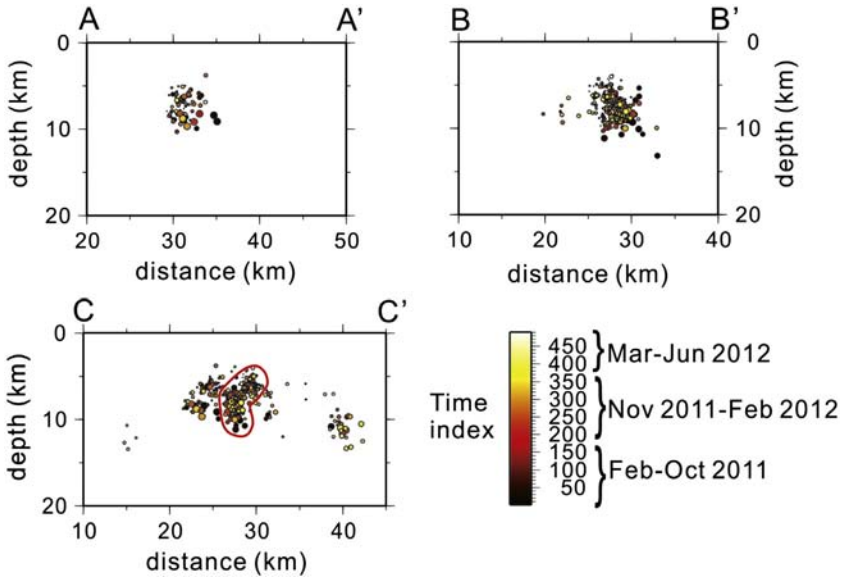

Fig. 6. Depth cross-sections showing the distribution of relative location hypocenters. The color scale given at the lower right hand side represents the index number of each event based on chronological order. The red curve delineates the two clusters that are located near the caldera rim between Nea Kameni and Thera islands. (For interpretation of the references to color in this figure legend, the reader is referred to the web version of this article.)

the entire period of the unrest, while THT1 covers the period after September 2011 and has the largest number of measurements (Fig. 7). As it can be seen most ratio values are below the background Vp/Vs value of 1.77 estimated by Dimitriadis et al. (2009) using a Wadati diagram. There seems to be an increase of the ratio during October and December 2011, followed by a new decrease thereafter. After February 2012 a trend of approaching the background Vp/Vs is visible, even though we cannot draw firm conclusions due to the paucity of observed values. It is worth noting that the only station that exhibits an average Vp/Vs value close to 1.77 is CMBO which lies to the north of most seismic sources.

4. Shear wave anisotropy

4.1. Measurement methodology

Shear wave splitting is the process where shear waves are split into two almost orthogonal polarizations which travel at different velocities (Crampin and Peacock, 2005, 2008). This process may be related either to the alignment of microcracks in response to the in situ stress field, or to aligned planar features such as fault zone fabrics. Two parameters are used to describe splitting, namely the orientation φ of the fast moving polarized wave and time delay δt between the two split shear waves. The former provides information about the direction of the maximum horizontal stress while the latter is a measure of the strength of anisotropy along the raypaths. Volcanoes represent places pervaded by numerous crack systems due to fluid circulation and also exhibit strong variations of stress conditions related to magmatic intrusions. A number of studies have shown that these variable stress conditions are reflected to changes in shear wave anisotropy parameters (Gerst and Savage, 2004; Bianco and Zaccarelli, 2009; Johnson et al., 2010; Savage et al., 2010; Unglert et al., 2011).

Table 1
Summary of measurements per station for the ratio of compressional to shear wave velocity for all events that had clear P- and S-phases. Nobs is the number of observations; Vp/Vs is the average value of the ratio and σ the standard deviation.

Station	Nobs	Vp/Vs	σ
THRA	128	1.56	0.18
SANT	65	1.54	0.12
THT1	166	1.48	0.14
CMBO	26	1.73	0.22
SAP2	51	1.58	0.18
SAP3	4	1.70	0.10
Total	440	1.54	0.17

We measure shear wave splitting parameters in our dataset by using the cross-correlation method (Ando et al., 1983). In this method the two horizontal seismogram components are rotated in the horizontal plane at 1 degree increment of azimuth α from -90 to 90°. Then for each azimuth the cross-correlation (CC) coefficient is calculated between the two orthogonal seismograms, for a range of time delays τ in a selected time window. When the absolute value of CC coefficient reaches a maximum the corresponding values α and τ are chosen as the fast polarization direction and the time delay of the slow shear wave respectively. The measurement uncertainty for a 95% confidence interval is estimated using a *t*-test for the values of CC coefficient (Kuo et al., 1994). Waveforms can be distorted by phase conversions in the case when they reach the surface at incidence angles larger than 35°. For this reason we select event-station pairs that correspond to incidence angles that are smaller than this value, or in other words are within the shear wave window.

We first integrate the waveforms to displacement and then bandpass filter between 1 and 10 Hz using a two-pole Butterworth filter. As has been mentioned previously, station THRA is a strong-motion sensor and its acceleration waveforms were first converted to displacement before filtering and extracting shear-wave splitting parameters. The measurement window for each waveform starts 0.05 s before the S-wave arrival while the endpoint is adjusted each time until the value of the CC coefficient between the slow and fast components becomes maximum. The reasoning behind this choice of window measurement is based on the fact that the suitable endpoint may actually vary with different waveform characteristics. We consider that a splitting measurement is valid only when it conforms to the following criteria (see also Liu et al., 2008): (1) the CC coefficient is larger than 0.80; (2) the signal-to-noise ratio is larger than 2.5; (3) the change of the measured δt is less than 0.02 s when the window size is varied by ± 0.02 s; and (4) the change of measured φ is less than 10° when the window size is varied by ± 0.02 s. All measurement results were visually inspected in order to ensure that there is no cycle skipping or other anomalous effects. In this way we were able to extract 73

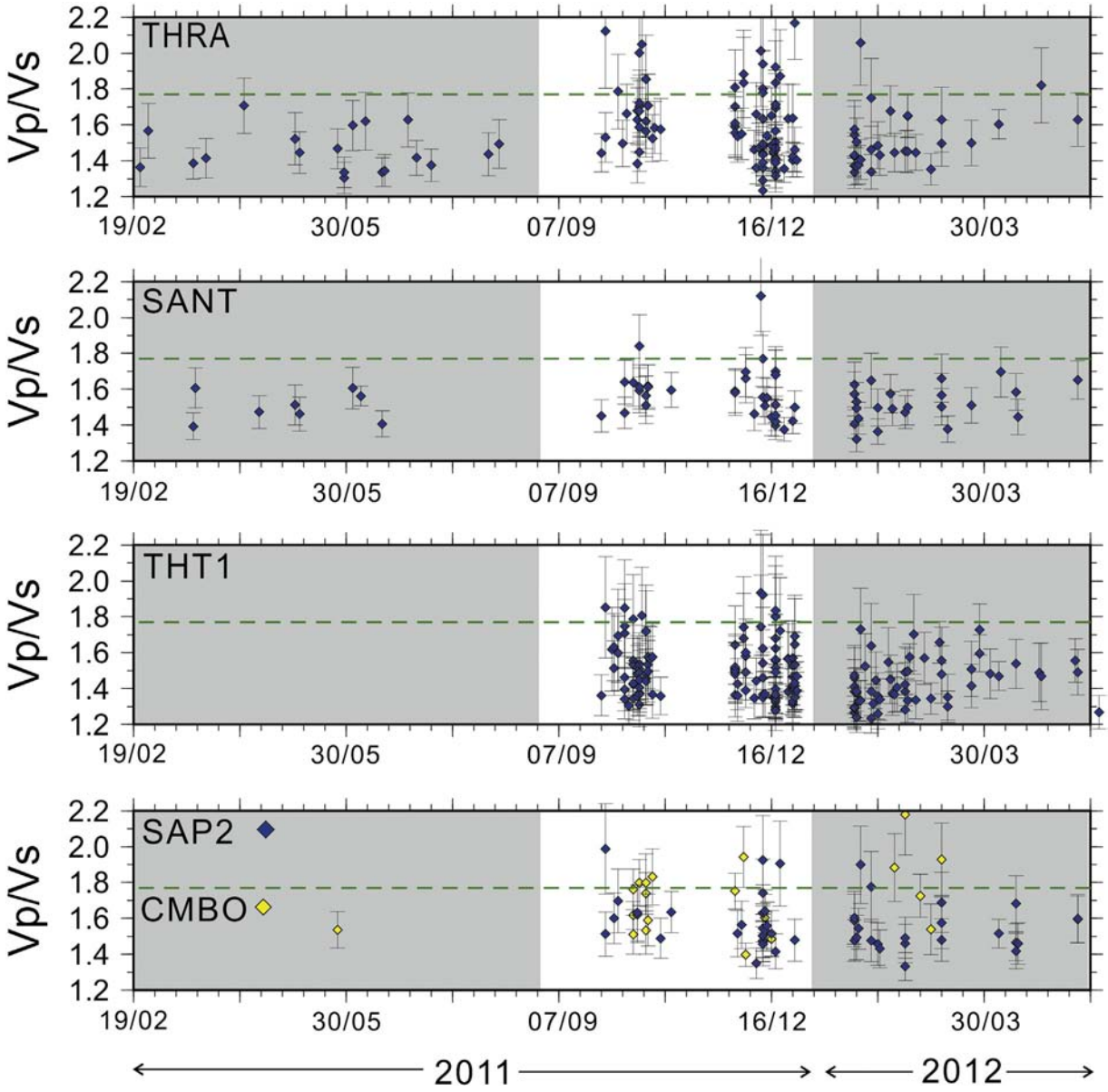

Fig. 7. Diagrams showing the variation of ray path averaged Vp/Vs ratio as a function of time for five different stations. The green line indicates the background Vp/Vs ratio (~1.77) for the Santorini area estimated by Dimitriadis et al. (2009). Shaded areas in each diagram highlight the three different deformation phases observed (see text for more details). Black vertical bars represent errors in measurement. (For interpretation of the references to color in this figure legend, the reader is referred to the web version of this article.)

splitting parameters and Fig. 8 shows an example of a valid splitting measurement.

These shear wave splitting observations may also be attributed to complex source mechanisms of the events or S-to-P conversions. The small magnitude of the analyzed events ($M_L < 3$) and the simplicity of the recorded waveforms give us confidence that the former suggestion is unlikely in our case. The latter explanation does not seem probable either, since this type of conversion shows the greatest amplitude on the vertical component, unlike our data where the maximum amplitude lies in the horizontals. The default explanation for the cause of crustal anisotropy is the presence of fluid-saturated cracks in the rock that are aligned parallel to the maximum horizontal stress direction (Crampin and Peacock, 2008). The dimensions of these cracks may vary considerably from microstructures to tens of meters, however, a larger size crack will also tend to significantly attenuate the propagating shear waves which is not observed in our dataset. Other causes of crustal anisotropy may also include aligned crystalline rocks such as the ones found in metamorphic complexes or fault zones. As we have no clear evidence in favor of such physical mechanisms, we interpret the shear wave splitting observed during the 2011 unrest as resulting from stress-aligned fluid-saturated microcracks.

4.2. Results

All of the valid splitting measurements we have derived concern the stations that are installed on Thera island (Fig. 9). The reasons for this are the following: (1) two of these stations (SANT, THRA) were installed prior to the unrest, resulting in the recording of many more events than other stations; (2) the stations on Thera had in general fewer gaps from data transmission malfunctions; and (3) owing to the distribution of seismicity many recordings at the stations in Nea Kameni and Therasia were outside the shear wave window. Table 2 summarizes the results for each station in terms of the number of observations, the mean value of φ based on circular statistics and mean/standard deviation for δt.

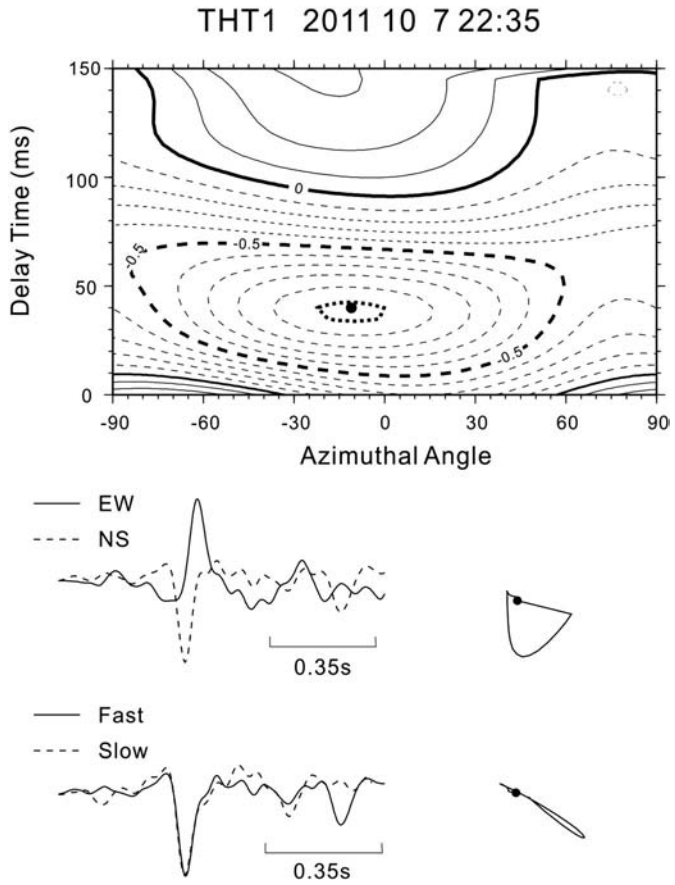

Fig. 8. A valid splitting measurement of an S-wave recorded at station THT1 for an event that occurred in October 7, 2011. Upper panel: diagram of the distribution of the cross-correlation coefficient in (φ, δt) space. The preferred solution corresponding to the maximum value (dot) is shown within the 95% confidence region (thick dotted line); dashed contours represent negative coefficients. Lower panel: upper two traces are the superposition of E–W and N–S components, while the lower two traces are the fast and slow components after correction for anisotropy. Particle motions are shown to the right of each sub-panel.

The fast polarization measurements exhibit two dominant directions, one along NE–SW and another one along NW–SE which in some cases coincides with the directions of the GPS velocity field. On the other hand, Dimitriadis et al. (2009) derived the stress tensor for the Santorini–Coloumbo area after inverting a set of earthquake focal mechanisms. The authors found that the regional stress is predominantly extensional with the σ_3 axis along the N311°E direction while the σ_2 axis, which represents the maximum horizontal stress σ_H, has a direction of N221°E. Therefore fast directions at stations THRA, SAP2 and THT1 seem to be influenced more by the regional stress field, in contrast to station SANT whose fast directions point inside the caldera at the location of the Mogi source. This difference can be explained by the fact that stations THRA, SAP2 and THT1 lie quite close to the observed uplift area where the vertical stresses exerted do not affect the maximum horizontal stress near the station. On the contrary, SANT is at such a distance from the area of uplift that the radial stresses exerted are stronger and perturb the crack orientations from the regional σ_H direction. A similar spatial variation of the fast polarization directions at stations near and far from the deforming area was observed at Okmok volcano, Alaska (Johnson et al., 2010).

Temporal variations of shear wave splitting parameters may also give clues to the dynamics of the deformation process, however, in order to obtain meaningful results any variations due to ray path differences have to be excluded. We searched our catalog of relocated events for the purpose of finding pairs of events, hereafter called "doublets" that are located very close to each other but have occurred at different times. Seven such doublets have been found with horizontal and vertical location differences of less than 600 m and hypocentral depths in the range of 5–8 km (Fig. 9). Fig. 10 shows plots of pairs of φ, δt and Vp/Vs measurements for each doublet as a function of time. Even though temporal variations of the fast polarization directions do not show any particular pattern, the variations in delay time and Vp/Vs ratio exhibit a clearly decreasing trend with time. More specifically, the delay time decreases significantly from 70 ms to less than 50 ms for the majority of doublets in the period from February to October 2011. This decreasing trend continues and from 50 ms in October 2011 most delay times assume a value of about 10 ms in February 2012. The Vp/Vs ratios show that from October 2011 until February 2012 all doublets exhibit variable amounts of decreases in Vp/Vs, while one doublet spanning the period October 2011 to April 2012 shows some increase. However, for some doublets the associated error in Vp/Vs estimation is larger than the observed variation.

5. Discussion

5.1. Deformation phases and temporal variations of Vp/Vs and δt

The evolution of deformation behavior during the 2011 unrest at Santorini caldera shows that uplift started in January 2011 exhibiting a peak in July–August of the same year, followed by a small subsidence thereafter and a new uplift peak between October–December 2011 until all deformation stopped in February 2012 (Foumelis et al., 2013; Lagios et al., 2013). As seen previously, these variations do not seem to directly affect the seismicity distribution, however the temporal changes of the Vp/Vs ratio at several stations roughly follow the timing of these deformation phases (cf. Fig. 7). In general, the Vp/Vs ratio of rocks depends on factors such as lithology, crack density, aspect ratio of cracks and the presence of fluids (Tatham, 1982; Dvorkin et al., 1999; Lin and Shearer, 2009). From these factors lithology is the least plausible as an explanation, since rock composition changes occur at much longer time scales than the variations of Vp/Vs observed here. Additionally, if we assume that the cracks are penny-shaped then the average Vp/Vs values for the three periods should correspond to crack aspect ratios within a rather limited range (~0.5–1) (Berryman et al., 2002). As the aspect ratio does not seem to vary considerably, it can be concluded that the fluid content is the most influential factor in determining the Vp/Vs observed variations.

Time-lapse seismic tomography in volcanic and geothermal systems was particularly successful in delineating bodies of high or low Vp/Vs ratio and in tracking their spatial/temporal changes (Gunasekera et al., 2003; Husen et al., 2004; Vanorio et al., 2005; Chiarabba and Moretti, 2006). These studies have highlighted the dominant role of fluids in influencing the values of Vp/Vs where liquids such as melt result in high Vp/Vs ratios (>1.8) by lowering the Vs, while gases shift the ratio to lower values (<1.7) as they affect more the P-wave velocity in the rock. In order to investigate in more detail the causes of the temporal variation of Vp/Vs during the 2011 Santorini unrest, we divided the estimated ratios into three periods following the deformation phases: January to August 2011, September to December 2011 and January to June 2012. Additionally, using the approximation of straight ray paths we calculated apparent Vp and Vs velocities for the same set of events that had an estimated Vp/Vs ratio. All of these quantities were averaged for each of the three periods and were compared to background values for the top 10 km of the crust derived from the minimum 1D velocity model of Dimitriadis et al. (2009).

Fig. 11 shows a summary of the results for each period along with the percentage of relative change from the background values. It can be seen that the Vp/Vs ratio during the initial deformation phase has a very low value that is 16.9% smaller than the background one (~1.77). During the second period the ratio increases but is still 11.8% smaller. Finally, in the last period it seems to decrease again on average, despite

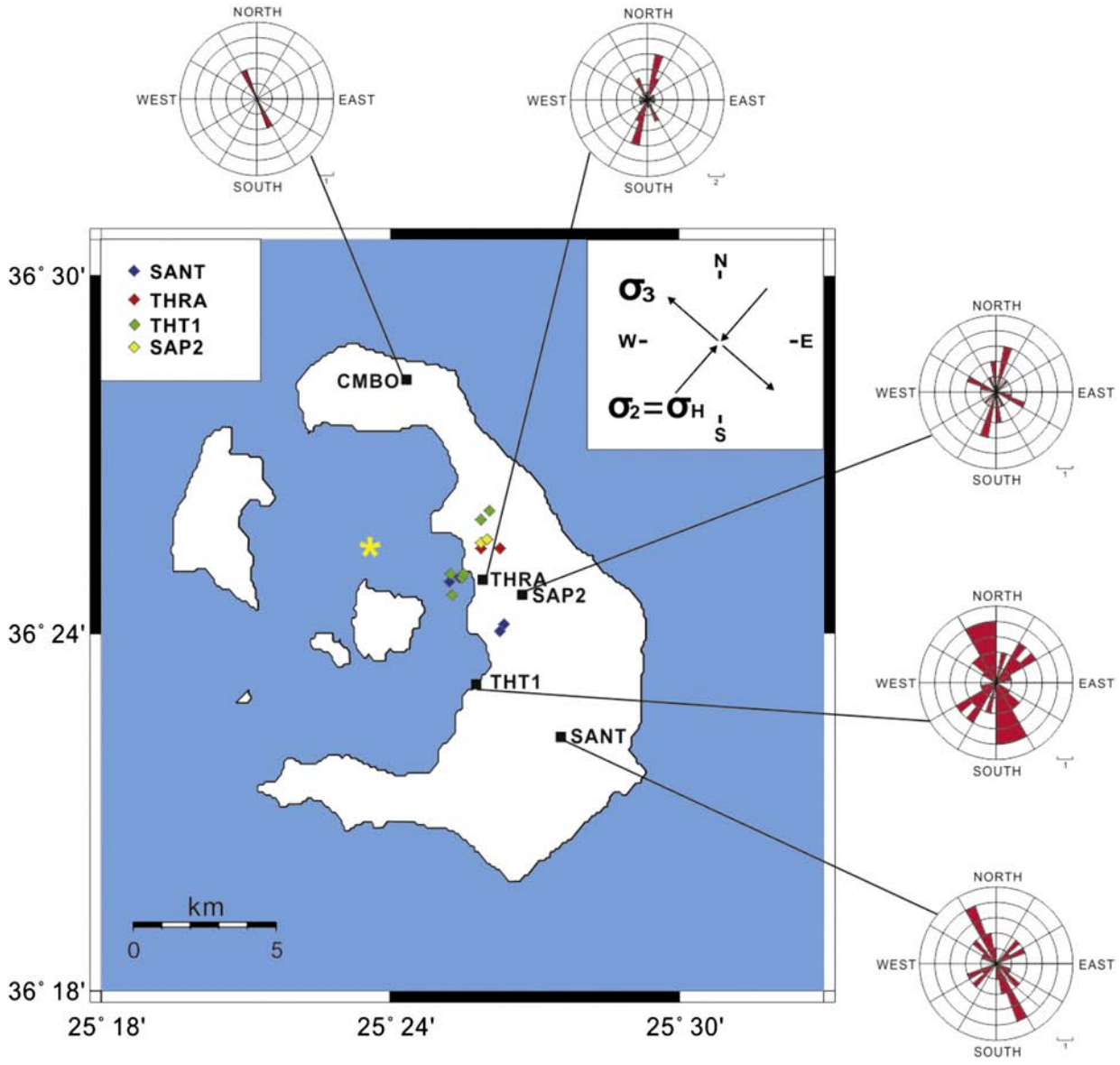

Fig. 9. Map showing the locations of the five stations where valid shear wave splitting measurements could be estimated along with the corresponding windrose diagrams. The diamond symbols represent the locations of the doublet events for the four different stations shown in the legend at the upper left hand corner. The inset diagram shows the orientations of the minimum and intermediate stress axes for the Santorini area derived by Dimitriadis et al. (2009). (For interpretation of the references to color in this figure legend, the reader is referred to the web version of this article.)

the fact that a few values after March 2012 tend to approach the background value. For the purpose of assessing whether these differences in Vp/Vs are indeed significant we performed a two-sample Kolmogorov–Smirnov test (Press et al., 1992). The test revealed that the difference in Vp/Vs values is significant at a 95% level for both the first and second, and second and third periods. The apparent velocities show that during all three periods Vp is affected more than the corresponding Vs, indicating the presence of a gas phase filling the cracks. At this point it should be noted that the majority of P- and S-wave ray paths whose travel-times were used to calculate Vp/Vs ratios, sample densely only the area between Thera and Nea Kameni. Therefore we cannot exclude the possibility that higher Vp/Vs values indicative of melt could be present in the northern part of the caldera. Based on these results, the temporal pattern that can be inferred has to do with a possible gas influx during January to August 2011 followed by some gas depletion from September to December 2011 and a new, but not as strong, influx of gas from January to June 2012. This interpretation is also supported by the temporal variations of anisotropic delay times as manifested by the doublets shown earlier. Large δt values occurred during the first period signifying high crack densities, thus allowing gases to occupy the space within cracks. This was followed by a progressive decrease of delay times suggesting closing of the cracks and escape of the gas resulting in the observed depletion.

Table 2
Summary of the shear wave anisotropy parameters measured for the Santorini dataset. Nobs denotes the number of observations per station, mean φ is the mean of the fast polarization directions based on circular statistics, δt is the delay times of splitting and σ is the standard deviation of these times.

Station	Nobs	Mean φ	δt (ms)	σ (ms)
SANT	16	352.5	42.8	±30.8
SAP2	10	343.3	41.5	±30.0
THRA	17	5.8	63.5	±37.7
THT1	29	3.9	32.2	±12.4
CMBO	2	336.5	72.5	±17.6

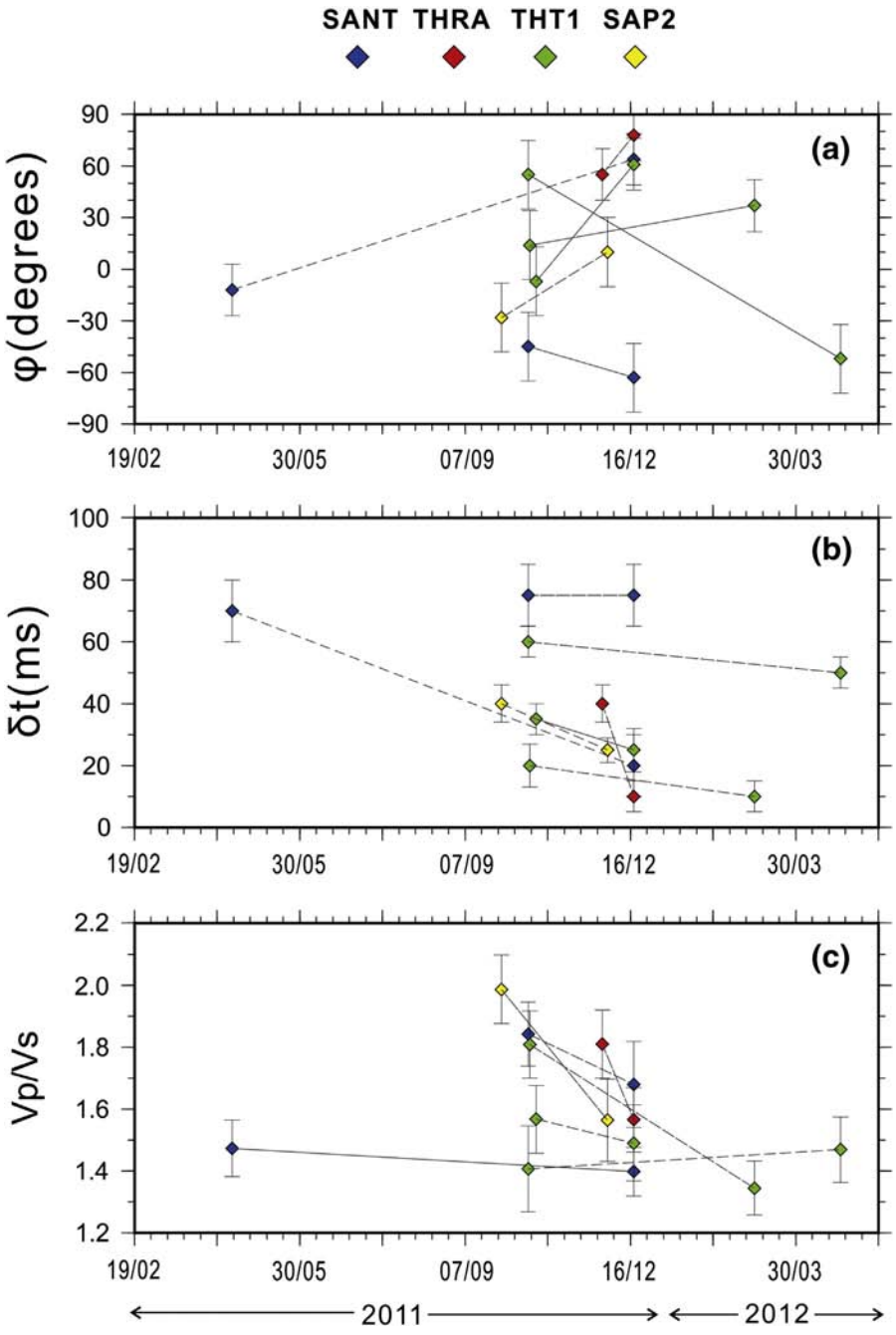

Fig. 10. (a) Diagram showing the variation of fast polarization direction for event doublets as a function of time, (b) the same for the delay time, and (c) the same for the Vp/Vs ratio. Black vertical bars represent errors in measurement for each of the three quantities. (For interpretation of the references to color in this figure legend, the reader is referred to the web version of this article.)

Recently, Tassi et al. (2013) published a study of geochemical changes in Santorini's fumarolic and submarine gas discharges during 2011–2012. Their observations agree well with the temporal variations in Vp/Vs and δt since they show a rapid increase of H_2 gas during the period July 2010 to May 2011 followed by a slowdown until a sharp drop is observed after February 2012. After H_2 concentration is diminished, other gases in the form of CO_2 and CH_4 exhibit considerable increase from February to July 2012. The authors also note that in the period from April to July 2012 gas samples show only minor air contamination, implying that the feeding conduits might be affected by self-sealing due to enhanced mineral deposition. Some of our anisotropy measurements exhibit fast direction orientations perpendicular to the dominant directions (cf. Fig. 9), hence they could represent "90-degree flips" which is thought to be an indicator of fluid overpressure (Crampin and Peacock, 2008). Most of these measurements occur after February 2012 and according to aforementioned observations they can be interpreted in terms of influx of CO_2 and CH_4 in obstructed conduits resulting in the buildup of overpressure.

5.2. Clues about the possible configuration of the volcanic system

The spatial distribution of relocated seismicity during the 2011 unrest presented here shows completely different characteristics from the distribution of routine locations extracted from the available catalogs. Rather than observing an elongated, NE–SW oriented cluster covering the Kameni islands, we derived a dense cluster of events delineating the western coast of Thera with other smaller clusters beneath the Kameni islands. While the interpretation of the former

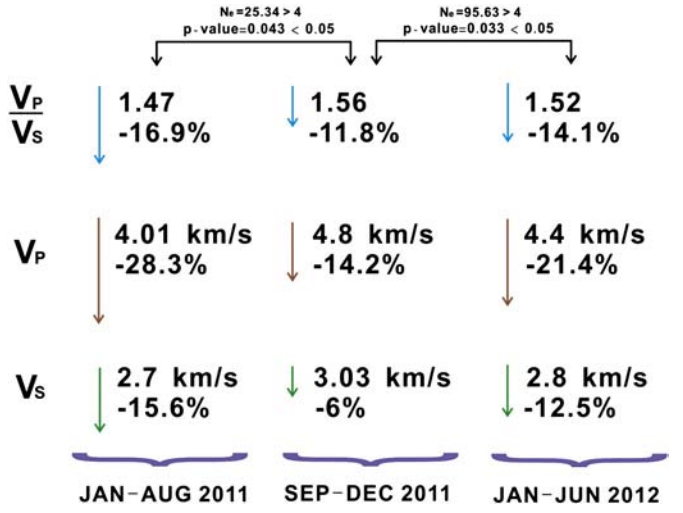

Fig. 11. Summary of the comparison between the average Vp/Vs ratio, apparent Vp, Vs velocities and the corresponding average background values derived from the minimum 1D velocity model of Dimitriadis et al. (2009). The percentage values given were calculated as the relative change of the two quantities. The p-value derived from the Kolmogorov–Smirnov two-sample tests is also shown and compared to the significance level (95%) where it can be seen that in both cases the p-value is always smaller, leading to the rejection of the null hypothesis. The quantity N_e is equal to $N_1 * N_2 / (N_1 + N_2)$ where N_1 and N_2 are the sizes of the two samples. N_e should be larger than 4 for the test results to be meaningful.

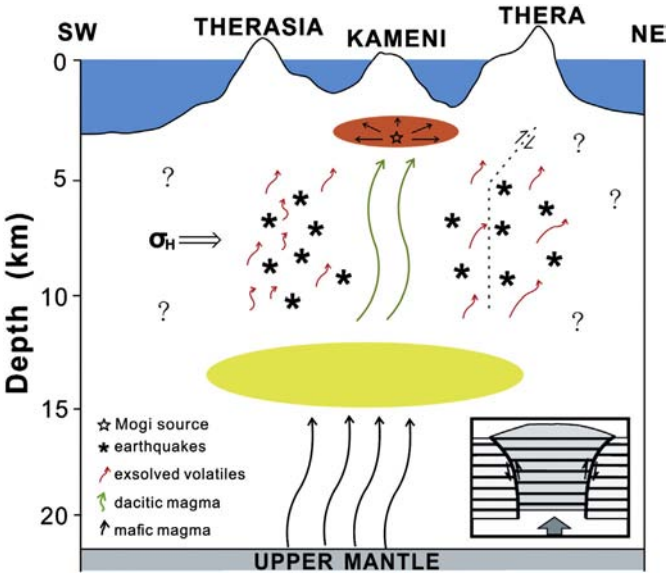

Fig. 12. Cartoon illustrating the possible configuration of the volcanic system beneath the Santorini caldera based on this and previously published studies. Mafic magma from the upper mantle moves into the deep reservoir (11–14 km) and differentiates to dacitic composition before it migrates to the shallower rhyolitic chamber. Its accumulation there causes the observed uplift and the reactivation of a preexisting ring fault. The inset shows the results of analog experiments where caldera resurgence leads to the reactivation of the bordering ring faults (after Acocella et al., 2000). Exsolved gases, or gases produced by chemical reactions with the surrounding rock may fill the open cracks generated by earthquakes. Their influx variations as a function of time could explain the observed periods of decreasing and increasing Vp/Vs ratios. (For interpretation of the references to color in this figure legend, the reader is referred to the web version of this article.)

observation would point to the well-known Kameni–Coloumbo line of regional extension (Pyle and Elliott, 2006), our results are suggesting the possibility that the main seismogenic structure during the unrest may be that of a ring fault along the caldera rim. Acocella et al. (2000) have performed analog modeling in order to investigate the effect of repeated cycles of resurgence and collapse on the faulting style at restless calderas. In the case of resurgence uplift that initiates a new cycle of deformation, as in the case of Santorini, the authors found that it resulted in the reactivation of preexisting ring faults. These ring faults border the resurgent block and consist of subvertical, slightly inward dipping surfaces (see inset of Fig. 12). The depth distribution of relocated events along the cross-section CC′ seems to agree with the predictions of this analog modeling (cf. Fig. 6).

Another interesting characteristic of the relocated events is the sharp cutoff in seismicity at depths above 5 km and below 11 km respectively. As earthquakes are the result of shear failure, their hypocenters can delineate the depth range where the crust is brittle and cold, while volumes devoid of seismicity may be interpreted as areas of a hotter and ductile crust possibly enclosing melt bodies. It has been long thought that the magma chamber beneath Santorini lies at depths shallower than 5 km (Barton and Huijsmans, 1986; Martin et al., 2008) which roughly coincides with the observed Mogi source depth. However, petrological models derived from the study of past eruption products suggest that a deep magma reservoir may also exist beneath the Kameni islands at depths between 10 and 14 km (Cottrell et al., 1999; Gertisser et al., 2009). The earthquake depth distribution presented here is compatible in general with such a configuration of one deep and another shallower reservoir.

Fig. 12 depicts the main elements of the volcanic system beneath the Santorini caldera based on the observations shown in this and previous studies. The magmatic system consists of two magma chambers at the aforementioned depths where the deeper one accepts inputs of mafic melt from the upper mantle. This melt resides in the reservoir and differentiates to dacitic composition before it moves upwards, entering the shallow chamber where it finally evolves to rhyodacitic melt before an eruption (Druitt et al., 2012). The melt movement results in the observed uplift due to its accumulation in the shallow reservoir and also in the redistribution of stresses within the brittle crust which is manifested by the generation of earthquakes. Additionally, any pre-existing structures such as ring faults may become reactivated as well. Seismogenesis is a particularly effective way of creating cracks that may subsequently serve as conduits for exsolved gases. Our observations, based on delay times from shear wave anisotropy, suggest high crack density during the first stage of deformation that is gradually diminishing towards the end of the unrest period possibly owing to stress relaxation and self-sealing of the crack system. Parks et al. (2012) have found that the total volume of material that has intruded during the 2011 unrest corresponds to about 10%–50% of the volumes of previous dome-forming eruptions in Santorini. Since this might highlight an increased probability of a future eruption, the need for a continuous monitoring of the caldera using all available geophysical and geochemical methodologies is dictated.

Acknowledgments

We would like to thank the National Science Council of Taiwan for the financial support of this study. Also we are grateful to all those scientists and scientific personnel at the National Observatory of Athens, Aristotle University of Thessaloniki and National and Kapodistrian University of Athens who helped to maintain and operate the seismic networks. The first author would like to thank Michelle Parks, Valerio Acocella, Tim Druitt and Georg Zellmer for stimulating discussions regarding Santorini's magma plumbing system. Constructive comments by two anonymous reviewers and the Editor-in-Chief Lionel Wilson significantly improved the original manuscript.

References

Acocella, V., Cifelli, F., Funiciello, R., 2000. Analogue models of collapse calderas and resurgent domes. J. Volcanol. Geotherm. Res. 104, 81–96.
Ando, M., Ishikawa, Y., Yamazaki, F., 1983. Shear wave polarization anisotropy in the upper mantle beneath Honshu, Japan. J. Geophys. Res. 88, 5850–5864.

Barton, M., Huijsmans, J., 1986. Post-caldera dacites from the Santorini volcanic complex, Aegean Sea, Greece: an example of the eruption lavas of near-constant composition over 2200 year period. Contrib. Mineral. Petrol. 94, 472–495.
Berryman, J.G., Pride, S.R., Wang, H.F., 2002. A differential scheme for elastic properties of rocks with dry or saturated cracks. Geophys. J. Int. 151, 597–611.
Bianco, F., Zaccarelli, L., 2009. A reappraisal of shear wave splitting parameters from Italian active volcanic areas through a semiautomatic algorithm. J. Seismol. 13, 253–266. http://dx.doi.org/10.1007/s10950-008-9125-z.
Bond, A., Sparks, R.S.J., 1976. The Minoan eruption of Santorini, Greece. J. Geol. Soc. Lond. 132, 1–16.
Carlino, S., Somma, R., 2010. Eruptive versus non-eruptive behaviour of large calderas: the example of Campi Flegrei caldera (southern Italy). Bull. Volcanol. 72, 871–886. http://dx.doi.org/10.1007/s00445-010-0370-y.
Chiarabba, C., Moretti, M., 2006. An insight into the unrest phenomena at the Campi Flegrei caldera from Vp and Vp/Vs tomography. Terra Nova 18, 373–379. http://dx.doi.org/10.1111/j.1365-3121.2006.00701.x.
Chouliaras, G., Drakatos, G., Makropoulos, K., Melis, N.S., 2012. Recent seismicity increase in the Santorini volcanic island complex. Nat. Hazards Earth Syst. Sci. 12, 859–866. http://dx.doi.org/10.5194/nhess-12-859-2012.
Cottrell, E., Gardner, J., Rutherford, M., 1999. Petrologic and experimental evidence for the movement and heating of the pre-eruptive Minoan rhyodacite (Santorini, Greece). Contrib. Mineral. Petrol. 135, 315–331.
Crampin, S., Peacock, S., 2005. A review of shear wave splitting in the compliant crack-critical anisotropic Earth. Wave Motion 41. http://dx.doi.org/10.1016/j.wavemoti.2004.05.006.
Crampin, S., Peacock, S., 2008. A review of the current understanding of seismic shear-wave splitting in the Earth's crust and common fallacies in interpretation. Wave Motion 45, 675–722. http://dx.doi.org/10.1016/j.wavemoti.2008.01.003.
Dimitriadis, I., Karagianni, E., Panagiotopoulos, D., Papazachos, C., Hatzidimitriou, P., Bohnhoff, M., Rische, M., Meier, T., 2009. Seismicity and active tectonics at Coloumbo Reef (Aegean Sea, Greece): monitoring an active volcano at Santorini volcanic center using a temporary seismic network. Tectonophysics 465, 136–149. http://dx.doi.org/10.1016/j.tecto.2008.11.005.
Druitt, T.H., Francaviglia, V., 1992. Caldera formation on Santorini and the physiography of the islands in the late Bronze Age. Bull. Volcanol. 54, 484–493.
Druitt, T.H., Costa, F., Deloule, E., Duncan, M., Scaillet, B., 2012. Decadal to monthly timescales of magma transfer and reservoir growth at a caldera volcano. Nature 482, 77–80. http://dx.doi.org/10.1038/nature10706.
Dvorkin, J., Mavko, G., Nur, A., 1999. Overpressure detection from compressional- and shear-wave data. Geophys. Res. Lett. 26, 3417–3420.
Evangelidis, C.P., Melis, N.S., 2012. Ambient noise levels in Greece as recorded at the Hellenic Unified Seismic Network. Bull. Seismol. Soc. Am. 102, 2507–2517. http://dx.doi.org/10.1078/01201.10319.
Foumelis, M., Trasatti, E., Papageorgiou, E., Stramondo, S., Parcharidis, I., 2013. Monitoring Santorini volcano (Greece) breathing from space. Geophys. J. Int. 193, 161–170. http://dx.doi.org/10.1093/gji/ggs135.
Gerst, A., Savage, M.K., 2004. Seismic anisotropy beneath Ruapehu volcano: a possible eruption forecasting tool. Science 306, 1543–1547.
Gertisser, R., Preece, K., Keller, J., 2009. The Plinian lower Pumice 2 eruption, Santorini, Greece: magma evolution and volatile behaviour. J. Volcanol. Geotherm. Res. 186, 387–406.
Gunasekera, R.C., Foulger, G.R., Julian, B.R., 2003. Reservoir depletion at the Geysers geothermal area, California, shown by four-dimensional tomography. J. Geophys. Res. 108, 2134. http://dx.doi.org/10.1029/2001JB000638.
Heiken, G., McCoy, F., 1984. Caldera development during the Minoan eruption, Thira, Cyclades, Greece. J. Geophys. Res. 89, 8441–8462.
Hill, D.P., Langbein, J.O., Prejean, S., 2003. Relations between seismicity and deformation during unrest in Long Valley Caldera, California, from 1995 through 1999. J. Volcanol. Geotherm. Res. 127. http://dx.doi.org/10.1016/S0377-0273(03)00169-0.
Husen, S., Smith, R.B., Waite, G.P., 2004. Evidence for gas and magmatic sources beneath the Yellowstone volcanic field from seismic tomographic imaging. J. Volcanol. Geotherm. Res. 131, 397–410. http://dx.doi.org/10.1016/S0377-0273(03)00416-5.
Johnson, J.H., Prejean, S., Savage, M.K., Townend, J., 2010. Anisotropy, repeating earthquakes and seismicity associated with the 2008 eruption of Okmok volcano, Alaska. J. Geophys. Res. 115, B00B04. http://dx.doi.org/10.1029/2009JB006991.
Klein, F., 2002. User's Guide to Hypoinverse2000, a FORTRAN Program to Solve for Earthquake Locations and Magnitudes. USGS Open File Report 02-171.
Konstantinou, K.I., Yeh, T.-Y., 2012. Stress field around the Coloumbo magma chamber, southern Aegean: its significance for assessing volcanic and seismic hazard in Santorini. J. Geodyn. 54, 13–20. http://dx.doi.org/10.1016/j.jog.2011.09.003.
Kuo, B.Y., Chen, C.C., Shin, T.C., 1994. Split S waveforms observed in northern Taiwan: implications for crustal anisotropy. Geophys. Res. Lett. 21, 1491–1494.
Lagios, E., Sakkas, V., Novali, F., Bellotti, F., Ferretti, A., Vlachou, K., Dietrich, V., 2013. SqeeSAR and GPS ground deformation monitoring of Santorini Volcano (1992–2012): tectonic implications. Tectonophysics 594, 38–59. http://dx.doi.org/10.1016/j.tecto.2013.03.012.
Lin, G., Shearer, P.M., 2006. The COMPLOC earthquake location package. Seismol. Res. Lett. 77, 440–444.
Lin, G., Shearer, P.M., 2009. Evidence for water-filled cracks in earthquake source regions. Geophys. Res. Lett. 36, L17315. http://dx.doi.org/10.1029/2009GL039098.
Liu, Y., Zhang, H., Thurber, C., Roecker, S., 2008. Shear wave anisotropy in the crust around the San Andreas fault near Parkfield: spatial and temporal analysis. Geophys. J. Int. 172, 957–970. http://dx.doi.org/10.1111/j.1365-246X.2007.03618.x.
Lucente, F.P., De Gori, P., Margheriti, L., Piccinini, D., Di Bona, M., Chiarabba, C., Agostinetti, N.P., 2010. Temporal variation of seismic velocity and anisotropy before the 2009 Mw 6.3 L'Aquila earthquake, Italy. Geology 38, 1015–1018. http://dx.doi.org/10.1130/G31463.1.
Martin, M.V., Morgan, D.J., Jerram, D.A., Caddick, M.J., Prior, D.J., Davidson, J.P., 2008. Bang! Month-scale eruption triggering at Santorini volcano. Science 321. http://dx.doi.org/10.1126/science1159584.
Matoza, R.S., Shearer, P.M., Lin, G., Wolfe, C.J., Okubo, P.G., 2013. Systematic relocation of seismicity on Hawaii Island from 1992 to 2009 using waveform cross-correlation and cluster analysis. J. Geophys. Res. 118, 2275–2288. http://dx.doi.org/10.1002/jgrb.50189.
Newhall, C.G., Dzurisin, D., 1988. Historical Unrest at Large Calderas of the World, US Geological Survey (1009 pp.).
Newman, A.V., Stiros, S., Feng, L., Psimoulis, P., Moschas, F., Saltogianni, V., Jiang, Y., Papazachos, C., Panagiotopoulos, D., Karagianni, E., Vamvakaris, D., 2012. Recent geodetic unrest at Santorini caldera, Greece. Geophys. Res. Lett. 39, L06309. http://dx.doi.org/10.1029/2012GL051286.
Nur, A., 1972. Dilitancy, pore fluids and premonitory variations of ts/tp travel times. Bull. Seismol. Soc. Am. 62, 1217–1222.
Papoutsis, I., Papanikolaou, X., Floyd, M., Ji, K.H., Kontoes, C., Paradissis, D., Zacharis, V., 2013. Mapping inflation at Santorini volcano, Greece, using GPS and InSAR. Geophys. Res. Lett. 40. http://dx.doi.org/10.1029/2012GL054137.
Parks, M.M., Biggs, J., England, P., Mather, T.A., Nomikou, P., Palamartchouk, K., Papanikolaou, X., Paradissis, D., Parsons, B., Pyle, D.M., Raptakis, C., Zacharis, V., 2012. Evolution of Santorini volcano dominated by episodic and rapid fluxes of melt from depth. Nat. Geosci. 1–6. http://dx.doi.org/10.1038/ngeo1562.
Press, W., Teukolsky, S.A., Vetterling, W.T., Flannery, B.P., 1992. Numerical Recipes in C. Cambridge University Press, Cambridge.
Pyle, D.M., Elliott, J.R., 2006. Qunatitative morphology, recent evolution and future activity of the Kameni Islands volcano, Santorini, Greece. Geosphere 2, 253–268. http://dx.doi.org/10.1130/GES00028.1.
Savage, M.K., Ohminato, T., Aoki, Y., Tsuji, H., Greve, S.M., 2010. Stress magnitude and its temporal variation at Mt Asama volcano, Japan, from seismic anisotropy and GPS, Earth Planet. Sci. Lett. 290, 403–414. http://dx.doi.org/10.1016/j.epsl.2009.12.037.
Shearer, P.M., 1997. Improving local earthquake locations using the L1 norm and waveform cross-correlation: application to the Whittier Narrows, California aftershock sequence. J. Geophys. Res. 102, 8269–8283.
Shearer, P.M., Hardebeck, J.L., Astiz, L., Richards-Dinger, K.B., 2003. Analysis of similar event clusters in aftershocks of the 1994 Northridge, California, earthquake. J. Geophys. Res. 108 (B1), 2035. http://dx.doi.org/10.1029/2001JB000685.
Shearer, P.M., Hauksson, E., Lin, G., 2005. Southern California hypocenter relocation with waveform cross-correlation, part 2: results using source-specific station terms and cluster analysis. Bull. Seismol. Soc. Am. 95, 904–915. http://dx.doi.org/10.1785/0120040168.
Tassi, F., Vaselli, O., Papazachos, C.B., Giannini, L., Chiodini, G., Vougioukalakis, G.E., Karagianni, E., Vamvakaris, D., Panagiotopoulos, D., 2013. Geochemical and isotopic changes in the fumarolic and submerged gas discharges during the 2011–2012 unrest at Santorini caldera (Greece). Bull. Volcanol. 75, 711. http://dx.doi.org/10.1007/s00445-013-0711-8.
Tatham, R.H., 1982. Vp/Vs and lithology. Geophysics 47, 336–344.
Unglert, K., Savage, M.K., Fournier, N., Ohkura, T., Abe, Y., 2011. Shear wave splitting, Vp/Vs and GPS during a time of enhanced activity at Aso caldera, Kyushu. J. Geophys. Res. 116, B11203. http://dx.doi.org/10.1029/2011JB008520.
Vanorio, T., Virieux, J., Capuano, P., Russo, G., 2005. Three-dimensional seismic tomography from P wave and S wave microearthquake travel times and rock physics characterization of the Campi Flegrei caldera. J. Geophys. Res. 110, B03201. http://dx.doi.org/10.1029/2004JB003102.
Vougioukalakis, G.E., Fytikas, M., 2005. Volcanic hazards in the Aegean area, relative risk evaluation, monitoring, and present state of the active volcanic centers. The south Aegean active volcanic arc: present knowledge and future perspectives. Dev. Volcanol. 7, 161–183.